The Development of Optimal Charging Protocols for Lithium-Ion Batteries to Reduce Lithium Plating

Upender Rao Koleti [1]*, Truong Ngoc Minh Bui[1], Truong Quang Dinh[1], James Marco[1]

[1] *WMG, The University of Warwick, Coventry CV4 7AL, United Kingdom*

Abstract

The study proposes two novel fast-charging strategies for lithium-ion batteries that prevent or minimize the occurrence of lithium plating. A new impedance tracking (IT) method that detects the onset of lithium plating is used to derive the charge profiles for both offline and online application at an ambient temperature of 20 °C for an NCA/graphite-based 18650 type commercial cell. Charging performance and capacity fade trends for the proposed charging strategies are evaluated against the standard constant current/constant voltage (CC-CV) charging profile. Experimental results indicate that the proposed strategies can extend the battery life by more than 75% when compared to the CC-CV profile with only a marginal increase in associated charge time.

Keywords: Lithium Plating; Fast Charging; Lithium-Ion; Impedance Tracking (IT), Battery Management System (BMS)

Terms and Abbreviations

Ah	Ampere Hour
BMS	Battery Management System
CC	Constant Current
CC-CV	Constant Current Constant Voltage
CTL	Charge Transfer Limitations
CV	Constant Voltage
DV	Differential Voltage
EIS	Electrochemical Impedance Spectroscopy
EV	Electric Vehicle
IT	Impedance Tracking
LAM	Loss of Active Material
LLI	Loss of Lithium Inventory
NE	Negative Electrode
NEP	Negative Electrode Potential
NCA	Lithium Nickel Cobalt Aluminium Oxide
OCV	Open Circuit Voltage
PE	Positive Electrode
SDL	Solid Diffusion limitations
SEI	Solid Electrolyte Interphase

* Upender Rao Koleti. Tel.:+44-7471114926; *E-mail address*: u.koleti@warwick.ac.uk.

SOC	State of Charge
SOH	State of Health
VRP	Voltage Relaxation Profiles
LFP	Lithium Iron Phosphate
NCA	Lithium Nickel Cobalt Aluminium Oxide
NE	Negative electrode
NEP	Negative electrode potential
NMC	Nickel Manganese Cobalt Oxide
PDE	Partial Differential Equation
SEI	Solid Electrolyte Interface
SPM	Single-particle model
SOH	State of Health
SOC	State of Charge
VRP	Voltage Relaxation Profile

Mathematical Notation, Symbols and Units

dI	Change in cell current, A
dV	Change in cell voltage, V
f_{max}	Frequency at which the reactance attains a maximum level in the semi-circle region of the EIS plot
f_{tr}	Frequency at which the impedance due to diffusion with a slope of 45° begins in the EIS
i	Control loop execution counter
I_{ch}	Charge current, A
n	Number of SOC measurement points in a charging event
V_1	Terminating voltage level at 1.5C charge rate, V
V_2	Terminating voltage level at 1.25C charge rate, V
V_3	Terminating voltage level at 1C charge rate, V
V_4	Terminating voltage level at 0.75C charge rate, V
V_i	Cell voltage at the i^{th} control loop execution counter, V
V_p	Cell voltage level prior to the charge interruption period, V
V_L	Cell voltage level at the end of the 0.5 s charge interruption period, V
Z_n	Impedance value measured at the n^{th} SOC measurement point, Ω
ZP_n	Impedance value predicted at the n^{th} SOC measurement point, Ω
Z_{tr}	Impedqance at the f_{tr}

1. Introduction

Electric vehicles (EV) are expected to play a crucial role in achieving a more environmentally sustainable form of mobility. However, the Li-ion battery used in these vehicles still poses many challenges. One such requirement is to extend battery life while maximizing both EV and charging performance [1]. A variety of ageing mechanisms such as solid electrolyte interface (SEI) growth on the negative electrode (NE) [2, 3], active material cracking at the electrodes [4], dissolution of transition metals from the positive electrode [5] and lithium plating on the NE [6] contribute to overall degradation with time and use. Therefore, minimizing each of these ageing mechanisms is essential in extending battery life.

It is often discussed that lithium plating is one of the major ageing mechanisms associated with fast charging [7, 8]. While charging at high charge currents and low temperatures, lithium metal depositions can begin to form on the NE particularly at a high state of charge (SOC) when the potential of the NE drops below the Li reference potential. Under the influence of lithium plating, as discussed within [9, 10], battery degradation is known to accelerate significantly.

Much research has been done to avoid or minimize the occurrence of lithium plating with the help of electrochemical modelling methods or new experimental approaches. With the electrochemical modelling of a battery [11, 12], the NE potential (NEP) is estimated and charging current is controlled accordingly to keep the NEP above the Li reference. However, these modelling methods have many challenges. First, extracting the electrochemical and physical parameters of the battery is difficult [13]. Second, the implementation of these models in a real-time context is difficult because of the complexity of their governing equations. Third, the accuracy of the NEP estimation as the battery ages depends strongly on the accurate representation of the ageing mechanisms present in the battery. Finally, parametrization of the model as battery undergoes degradation is difficult for many practical systems [14, 15].

While the experimental based charge control approaches rely on the influence of lithium plating on the battery ageing or the NEP measurement or the detection of lithium plating occurrence. By measuring the Coulombic efficiency at various charge rates, an optimum C-rate that minimizes the degradation from lithium plating and other ageing mechanisms is identified [16]. Similarly, the charge rate is selected from the empirical ageing and equivalent circuit models developed from the life tests conducted at different temperatures and charge rates [17, 18]. The concern with these approaches is they fail to adapt the charge profile to battery ageing as lithium plating tendency is known to change with battery age [14, 19]. When it comes to the NEP measurement-based control, use of a three-electrode cell to monitor the NEP and to derive a charging profile can be found from the literature [9, 20]. However, the transferability of the results obtained from the developed or modified cell to the corresponding commercial cell is difficult because of the extraction process of electrodes, use of a different electrolyte and cell construction compared to the commercial cell.

On the other hand, in-situ lithium plating detection methods such as neutron diffraction [21], the use of differential voltage curves [14, 22] and Voltage Relaxation Profile (VRP) methods [6, 23] can be utilized to identify a charge profile that reduces lithium plating levels. These methods are based on the intercalation/de-intercalation of the reversible part of lithium plating that modifies the electrode lithiation levels and changes the cell terminal voltage. However, they are

sensitive to the value of cut-off current used in the CV phase of the charging profile [24]. Further, these methods often fail to detect the onset of lithium plating during the charging process, therefore limiting their ability to minimize the lithium plating amount.

In contrast to the existing detection methods of lithium plating, it is shown recently that a new impedance tracking (IT) method can detect the onset of lithium plating while the battery is still in charge and at practical working conditions such as ambient temperatures higher than 10 ^{o}C [25]. The influence of lithium plating induced side reactions on the charge transfer limitations (CTL) can be identified by tracking the battery impedance. Interruption of CC charging for a short period every one per cent SOC rise allows tracking the impedance arising from the CTL. Under the influence of lithium plating, the impedance profile shows a deviation from its usual plating free or low C-rate charging profile. This allows detection of the onset of lithium plating. A full description of the IT method is discussed in [25] and will therefore not be repeated here. However, a brief overview of underpinning theory is discussed in section 3.

In this study, we introduce how the IT method can be implemented into battery charging control to derive online and offline charge profiles. The offline charge profile that employs a pre-characterization procedure and the online charge profile that defines the self-regulating charge current are detailed. The online approach is implemented and verified on a microcontroller-based evaluation board to better define its applicability for real-time use. The impact of the modified charge profiles on the charging performance and battery life are evaluated against the standard constant current - constant voltage (CC-CV) charge profile.

This paper is structured as follows: In Section 2, the experimental plan and test setup are discussed. Section 3 presents the procedures followed in deriving the charge profiles. Section 4 discusses the test results and further analysis. Overall conclusions of this research and outlines for the future work are given in Section 5.

2. Experimental Approach

The commercial 18650 format cells tested in this study have a nominal capacity of 3 Ah and a cell voltage range of 2.5 - 4.2 V. Negative and positive electrodes of the cells consist of graphite and NCA, respectively. The cells are characterized and cycled inside a climate chamber (Binder 9020-0385) along with a liquid cooling system (LAUDA) providing a stable ambient temperature (20 °C) with an accuracy of ±1 ^{o}C. In this study, three types of charging profiles at 20 °C are studied Three cells are used for each profile to ensure the robustness of the results obtained.

- Set A: Cycling with standard CC-CV protocol
- Set B: Cycling with offline optimized charging profile
- Set C: Cycling with online optimized charging profile

In case of the CC-CV charge profile, the cells are charged at a constant current of 3 A (1C) until a cell voltage of 4.2 V is reached, followed by a constant voltage (CV) phase until the current reduces below 1 A (1/3 C). To reduce the test duration and to be able to detect lithium plating using the VRP method besides the IT method, the CV phase cut-off

current during the charge is kept at such a high level. As discussed within [24], the use of low CV cut-off currents (< C/6) reduces lithium plating available for detection in the post-charge conditions as lithium stripping begins in the CV phase itself.

For the offline and online charge profiles (Sets B and C), the CC phase is replaced by a multi-stage CC profile where charge begins with a rate of at 1.5C and then the charge rate reduces gradually to a value of 0.5C in steps of 0.25C.

The Charge profile in the proposed (online and offline) strategies along with that of the CC-CV are described in Table 1. Offline and online charge strategies use different approaches as described in the latter part of this section to identify the cell voltages (V_1 to V_4) corresponding to these transition points in charge current. Irrespective of the charge profile, all the cells during cycling are discharged with a 1C current to a value of 2.7 V followed by a CV phase at 2.7V with a 0.1 A cut-off current. Such a low CV cut-off current reduces the influence of impedance on reaching the end of charge (EoC).

Table 1: Charge parameters for cycling experiments with the proposed and CC-CV charging protocols. All the cells are discharged with a 1C rate current to 2.7 V followed by a CV phase at 2.7V with a 0.1 A cut-off current.

Cell Set	Protocol name	Number of cells	Test case/Objective
Set A	CC-CV	3	CC charge (1C) until 4.2V ›› CV charge until I < 1 A
Set B	Offline	3	CC charge (1.5C) until V_1 ›› charge (1.25C) until V_2 ›› charge (1C) until V_3 ›› charge (0.75C) until V_4 ›› charge (0.5C) until 4.2 V ›› CV charge until I < 1 A
Set C	Online	3	

In the case of CC-CV and offline protocols (for Set A and Set B cells), a predefined charge profile is written to the Maccor test program for cycling the cells. For the offline protocol, the fixed-voltage levels (or transition voltages, V_1 to V_4 defined in Table 1) at which the charge rate is reduced are identified with an iterative pre characterization procedure using a separate five sets of new cells (referred as OFF1, OFF2, OFF3, OFF4 and OFF5 sets).

Table 2 shows the experimental parameters and objectives for the pre characterization tests which are conducted with the Maccor and the Lauda system. To derive the impedance profile during charge and to identify the onset of lithium plating, all the cells in the pre-characterization tests are interrupted for 0.5 s every 1% SOC increase during the CC charge phase. The reasons for selecting the time as 0.5 s and its ability to track the impedance from the charge transfer limitations and thus detect the onset of lithium plating can be found in detail within [25]. The procedure to identify the transition voltage levels in sequence and their application to the next set of cells are detailed in section 3.2.

Table 2: Offline characterisation test cases

Test sequence	charge Conditions	Test case	Objective
1	CC Charge(1.5C) to 4.2V	Set OFF1: 3 cells	To identify V_1
2	CC charge (1.5C) until V_1 ››› charge (1.25C) until 4.2 V	Set OFF2: 3 cells	To identify V_2
3	CC charge (1.5C) until V_1 ››› charge (1.25C) until V_2 ››› charge (1C) until 4.2 V	Set OFF3: 3 cells	To identify V_3
4	CC charge (1.5C) until V_1 ››› charge (1.25C) until V_2 ››› charge (1C) until V_3 ››› charge (0.75C) until 4.2 V	Set OFF4: 3 cells	To identify V_4
5	CC charge (1.5C) until V_1 ››› charge (1.25C) until V_2 ››› charge (1C) until V_3 ››› charge (0.75C) until V_4 charge (0.5C) until 4.2 V	Set OFF5: 3 cells	To verify that the derived charge profile avoids/minimizes plating

The online charge profile, applied to set C cells, tracks the impedance using the 0.5 s charge interruption for every 1% SOC increase and determines the plating onset and thus transitions between voltage levels (V_1 to V_4) in real-time. A microcontroller-based electronic system (TI evaluation board: C2000 Launchpad) with a cycle time of 10 ms is designed to track the impedance and to determine the voltage levels (V1 to V4) with the support of monitored cell voltages. Cell voltage signals of the cells in the online protocol are input to the TI board through voltage isolator evaluation modules (ISO224EVM) to maintain electrical isolation between the cells. The algorithms in the TI board tracks the cell voltage changes during the charge interruption periods to calculate the impedance for each 1% SOC increment and identifies the onset of lithium plating from the impedance profile. The procedures to calculate the impedance and identify the onset of lithium plating is detailed in section 3.3. Once the onset of plating is identified at each CC stage from the impedance values collected so far in that CC stage, the TI board communicates with the Maccor cycler through a Controlled Area Network (CAN) bus to initiate the charge rate reduction to the next CC level. Table 3 defines the CAN communication from the TI controller. To minimize the influence of charge interruptions on the comparison of degradation and to track lithium plating tendency over the cycle ageing, the 0.5 s charge interruption for every 1% SOC increment in the cc phase is applied to the cells in the CC-CV protocol as well.

Table 3: CAN communication specifications

Message	Sample rate	Data size	Data rate	Source	Target
Cell voltage	50 ms	16 bit	500 kbps	TI controller	Computer
Impedance	For every 1% SOC rise	16 bit	500 kbps	TI controller	Computer
Charge control	1 s	8 bit	500 kbps	TI controller	Maccor cycler

To compare the capacity change during cycling, ageing is interrupted once every twenty cycles. During these capacity tests at 20 °C, CC-CV charging and discharging at 0.5C with a 50 mA cut-off current at the CV stage is performed to quantify comparable values of capacities across all the cells under test. The same ambient temperature for cycle ageing and capacity tests are applied to reduce the experimental time as a soaking time of up to 4 h is typically employed when the ambient temperature is changed to ensure the cells have reached thermal equilibrium [26].

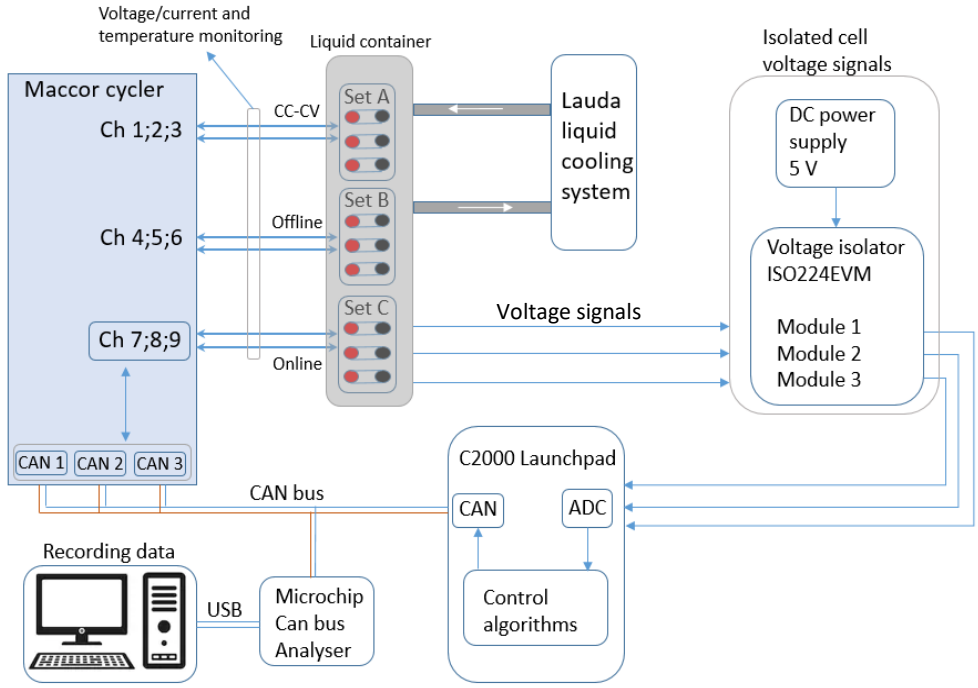

Figure 1: A single line diagram of the cycling experiments with the three charge protocols

The schematic diagram of the experimental setup for the cycling experiments is presented in Figure 1. A Maccor cell cycler (Model: Series 4000) is used to charge/discharge the cells. The Maccor unit enables the measurement of the cell voltage and current with an accuracy of ± 1 mV and ± 1 mA respectively. K-type thermocouples with an accuracy of ± 1 °C are attached on the axial surface of each cell to measure the cell surface temperature. Cells are installed within a manifold and liquid surface cooling used to maintain cell temperature at the desired value of 20 °C using a LAUDA controller (Model: Proline RP 845 C) with the ability to regulate temperature to an accuracy of ± 0.1 °C.

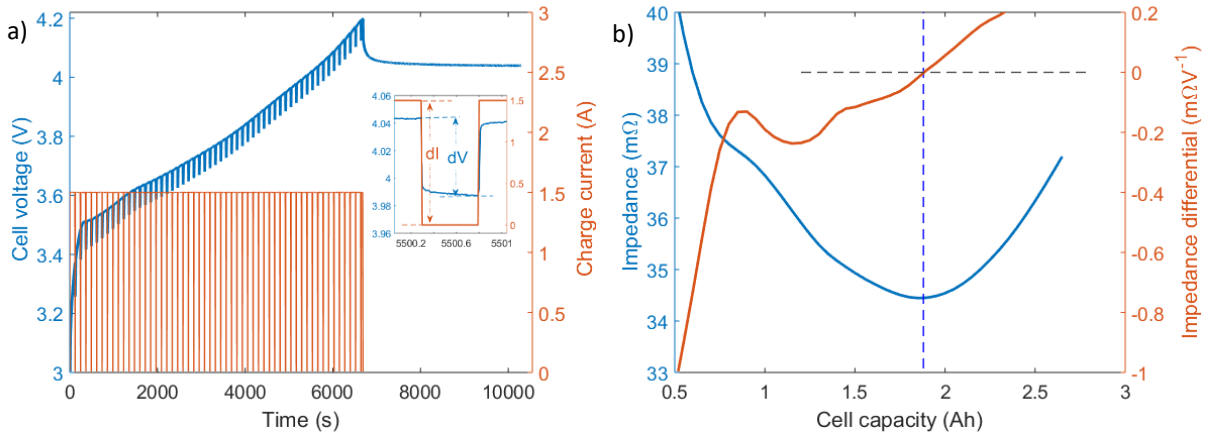

Figure 2: Charging at 0.5C rate: a) cell voltage and charge current and b) Impedance and its differential

3. Derivation of Charge Profiles

3.1. Impedance profile in the absence of plating

Before the 1.5C characterization, the cells in the OFF1 group are characterized for the impedance profile during the charge at 0.5C which is within the manufacturer recommended charge limits to identify the impedance profile under a plating free charge rate. Figure 2a shows the cell voltage and current during charge with the 0.5 s charge interruption every 1% SOC increase. As shown in the inset figure, the voltage difference (dV) between the cell voltage levels recorded before and at the end of an interruption is used for calculating the impedance (Z=dV/dI where dI represents the change in the current level, for example, dI is 1.5 A at 0.5C charge rate). The calculated impedance and its differential are shown in Figure 2b. During charge at 0.5C rate, the impedance in the early part of charging is found to reduce until it reaches a minimum level in the mid-SOC levels before it begins to rise in the latter part of charging. Corresponding impedance differential shows a reducing negative rate until it reaches zero level and then rising positive rates as the charge progresses. As discussed within [25], such an impedance profile indicates the absence of lithium plating. In contrary, at higher charge rates, such as 1C, that can cause lithium plating, the impedance profile shows a second negative trend in the latter part of charging in addition to the one in the early part of the charging process. This phenomenon is discussed further in the next section.

3.2. Identification of offline charge profile

In the proposed offline charging protocol, the multi-stage CC with monotonic decreasing charge C-rates (1.5C, 1.25C, 1C, 0.75C and 0.5C) is applied. To identify the cell voltage levels corresponding to these transitions, a sequential characterization procedure is employed using the IT approach.

First, the transition voltage level V1 is identified using the cells in the OFF1 set. Figure 3a shows the cell voltage and current profiles during the charge. Figure 3b shows the corresponding calculated impedance and its differential. The impedance profile shows a second negative trend after the charge level has increased beyond 1.4 Ah similar to the one at the start of charging. As discussed within [25], under the influence of lithium plating, the impedance profile that deviates from the usual “bath-tub” profile and shows a second negative trend indicates the occurrence of lithium plating and can be used be to identify the onset of plating. The impedance differential is used to identify the cell voltage where the second negative trend begins that infers the onset of lithium plating. At the cell voltage level of 3.936 V for a cell in OFF1 set, the impedance differential reached a minimum level (-0.021 mΩ/V) and then started to rise once again in the negative direction, unlike the rising positive rate of change as in the case of 0.5C charge rate. For the other two cells, these levels are identified as 3.941 and 3.943 V respectively. Therefore, an average level of 3.94 V is taken as the plating onset voltage (V_1) at 1.5C charge rate.

Next, with the identified V_1 from the OFF1 cells, the fully discharged OFF2 cells are charged with 1.5C charge rate until the cell voltage reached 3.94 V and then a 1.25C charge rate is applied for further charging until 4.2 V as shown in Figure 3c. Corresponding Impedance and its differential profiles are shown in Figure 3d. After reducing the current at 3.94 V by 0.25C, the impedance started to rise thus leading to levels of a positive rate of impedance differential in the initial phase of the second stage CC. The arrest of the negative trend and its rise as the charge progresses at the reduced CC rate indicates plating onset is avoided at 3.94 V. As the charge continues towards 4.2 V at the reduced 1.25C rate, the

impedance profile once again turned to negative trend indicating the onset of plating. Cell voltage level corresponding to the zero levels of the impedance differential and beyond which the impedance differential is negative is identified as 3.969 on a cell. An average level of 3.969 V from the three cells (3.969, 3.972 and 3.967 V) is taken as the plating onset voltage (V_2) at 1.25C charge rate.

Further, with the previously identified V_1 and V_2, a three-stage CC charging (1.5C until 3.94 V- 1.25C until 3.969 V -1C until 4.2 V) is applied to the cells in OFF3 set as shown for a cell in Figure 3e. Corresponding impedance and its differential can be found from Figure 3f that show the onset of plating at a later stage. From the three cells in OFF3 set, the average value for V_3 is found as 3.981 V similar to the procedure as mentioned for 1.5C-1.25C.

The results from the OFF3 are then used to define a 4 stage CC (1.5C-1.25C-1C-0.75C) with V_3 as the transition voltage for dropping the charge rate from 1C to 0.75C as shown in Figure 3g. The delayed plating onset voltage is now identified at a cell voltage level (V_4) of 4.038 V from the OFF4 cells using the impedance and its differential as shown for a cell in Figure 3h. Therefore, V_4 marks the transition of charge rate to 0.5C from 0.75C.

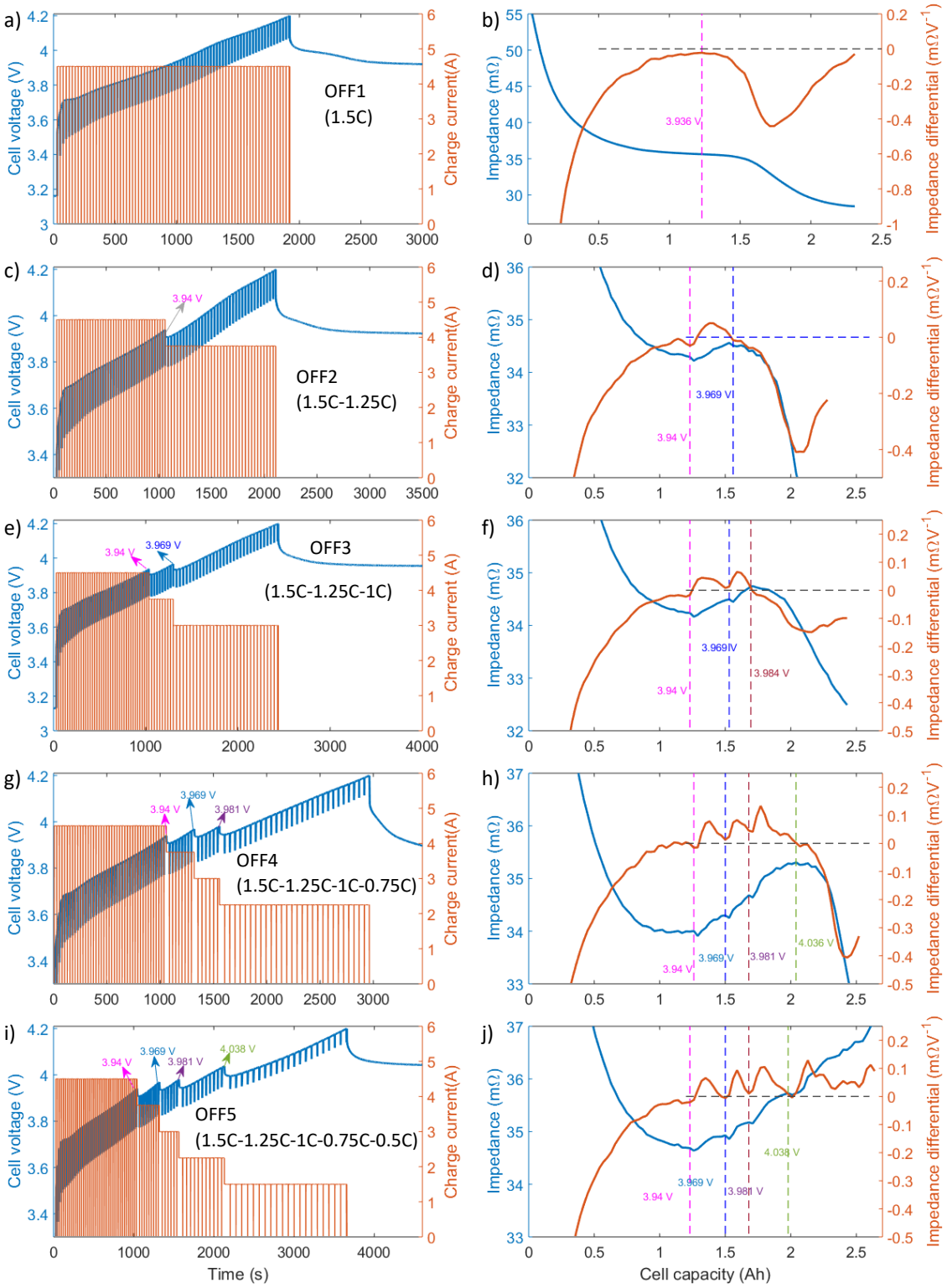

Figure 3: Offline charge profile development: Cell voltage and charge currents for different charge profiles and their corresponding impedance profiles and its differential

A five-stage CC charge profile with the transition levels at V_1, V_2, V_3 and V_4 (as seen from Figure 3i) is then applied to the cells in the OFF5 set to verify whether the derived profile can avoid lithium plating. The impedance and its differential as seen from Figure 3j show no further negative trend. This charging profile is summarized in Table 4 and is used for ageing experiments of the cells in the offline protocol.

Table 4: Offline profile: Identified voltage thresholds

CC stage	**Charge rate**	**Terminating voltage (V)**
1	1.5C	3.94
2	1.25C	3.969
3	1C	3.981
4	0.75C	4.038
5	0.5C	4.2

3.3 Online charge procedure

Similar to the offline profile, charging in the online procedure commences at 1.5C rate and then reduces to 0.5C in steps with a step size of 0.25C. At each CC stage, C-rate drop is initiated when the onset of plating is detected. To identify the plating onset and reduce the charge C-rate online in a charging event, the impedance values acquired by the TI board so far in that charging event are used. A simple flow chart to describe the algorithm developed for the microcontroller is presented in Figure 4 and described in the following sections.

3.3.1 Impedance calculation

The cell voltage is monitored every 10 ms is the single input for the TI board from which the impedance is calculated in multiple steps. First, during charge, the algorithm checks for the charge interruptions as the cell voltage rise from 2.75 V to 4.195 V. Since these cells have an Ohmic resistance of circa 25 mΩ, charge interruptions with a current of 1.5 A (or 0.5C) or more shall produce a minimum instantaneous voltage drop of more than 37.5 mV. To measure the voltage, the inbuilt 16 bit analogue to digital converter (ADC) of the TI controller is used which measures the cell voltage within ±0.4 mV accuracy and with a resolution of 68 µV. For each voltage measurement (v_i) an average of thirty-two samples are taken to further reduce the noise to ±0.05 mV. Here, i defines the control loop or the algorithm execution cycle counter that increases once in 10 ms. When a minimum voltage drop of 30 mV is detected from the last two voltage measurements (v_{i-1}-v_i), the charge interruption is detected. The voltage levels taken before the interruption (V_P) and at the end of 0.5 s interruption (V_L) are then recorded. Next, the impedance is calculated. With the known current change (dI) and the measured voltage change ($dV=V_P-V_L$), the impedance Z_n is calculated where n denotes the impedance count in the current charging event. Since the charge rate in each cycle begins with 1.5C as per the test program written to the Maccor and a transition executed by the Maccor to the next lower C-rate at any CC stage is controlled by the TI board, current C-rate and change in the charge current dI is assumed to be known and is not monitored by the TI board for simplicity. In real-time applications, both dV and dI can be directly calculated as the BMS typically monitors the cell voltage and cell current. However, it is noteworthy that for many applications these values do not define the voltage

and current for an individual cell, but rather the parameters across a single parallel connection of cells within the module or pack. With a minimum voltage difference of 50 mV and a current change of 1.5 A observed at 0.5C, error in the impedance calculation is estimated to be within 0.22 % (±0.1 mV error for the voltage difference of 50 mV and ±1 mA accuracy maintained by the Maccor for charge currents up to 5 A) of the actual value. Figure 5 shows the comparison of impedance profiles obtained from the Maccor data and that calculated by TI board while performing OFF5 characterization on a cell where the TI data is found to be within ±0.07 mΩ (< ±0.2%) of the Maccors data throughout the multi CC charging profile.

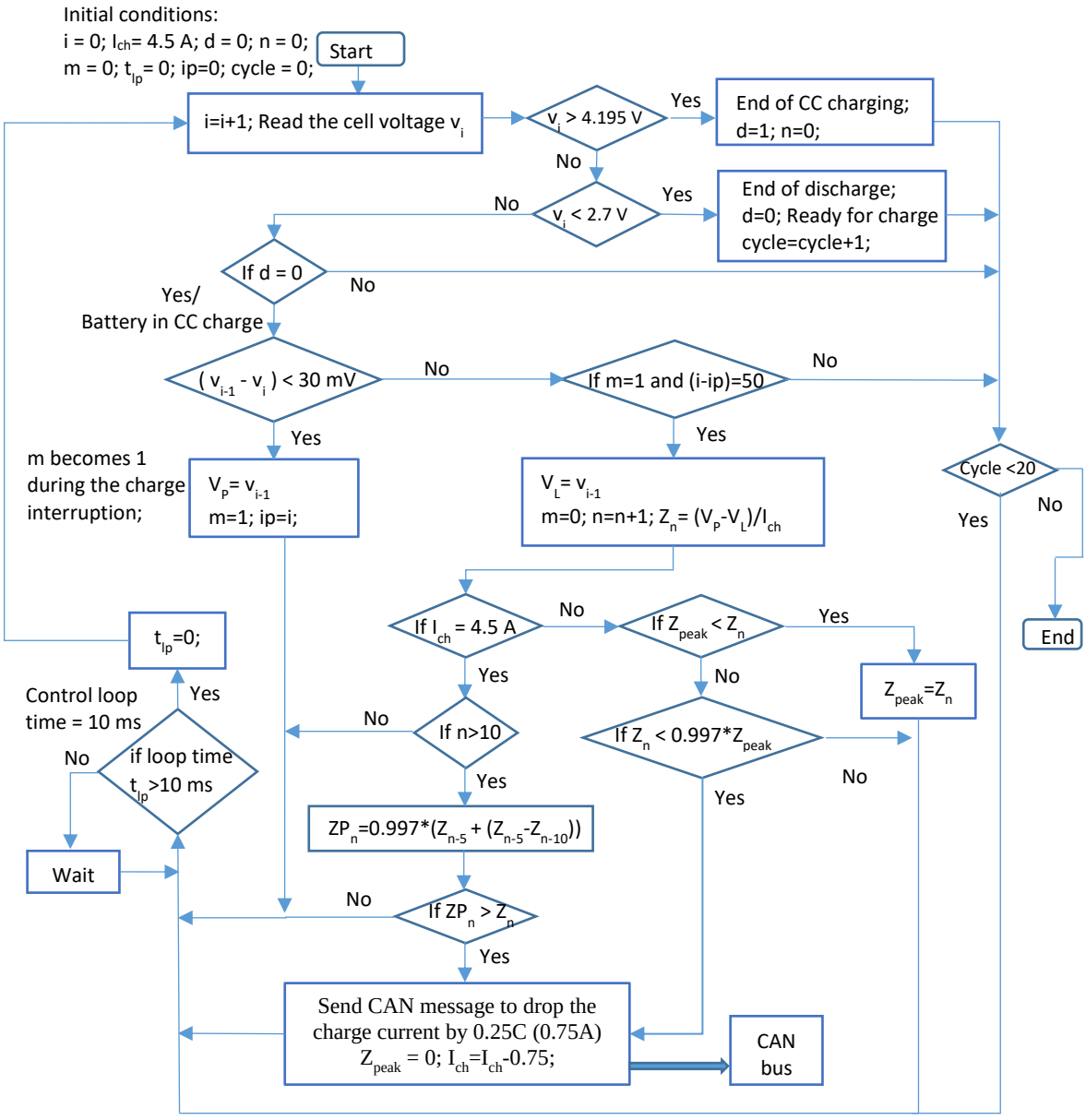

Figure 4: Flow chart representation of the online control algorithm

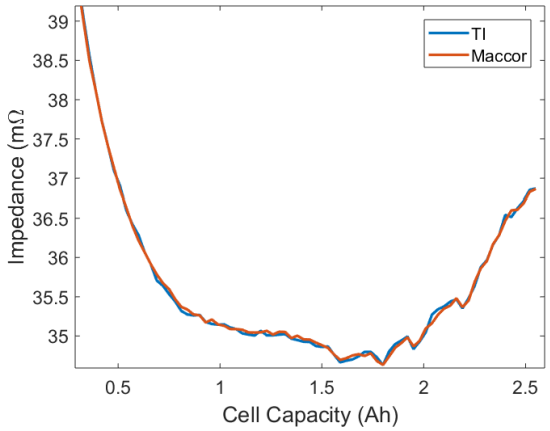

Figure 5: Impedance profiles obtained from the Maccor data and calculated by the TI controller

3.3.2 Detection of lithium plating onset

A closed-loop algorithm is designed to detect the onset of lithium plating during charge with the impedance values acquired so far within that charging event. Two different detection procedures are employed, one for the first CC stage (1.5C) and the other one for the remaining CC rates (<=1.25C) as described here. Once the SOC rises beyond 10% (or n>10 where n defines the number of SOC measurement points) at the initial charge rate of 1.5C, the past ten impedance values are used to verify the onset. Since the impedance has a reducing negative rate of change in the absence of plating, extrapolating the impedance using the past data (see eq 1) and their rate of change to predict the current impedance value (ZP_n) at any point of charge shall always produce a value which is lower than the actual value (Z_n). Once lithium plating commences, the Z_n value that drops from its plating free level goes blow the ZP_n value. Considering the impedance accuracy of 0.22%, a 0.3% margin is provided when comparing the predicted and actual values as shown here:

$$Plating\ is\ onset\ if\ ZP_n > Z_n \qquad (1)$$

$$here, ZP_n = 0.997 * (Z_{n-5} + (Z_{n-5} - Z_{n-10}))$$

Within a real-world application, this value may form one of the calibrations variables within the charging strategy. Application of this detection approach to detect plating onset is demonstrated with the data acquired from a cell in the OFF1 characterization as shown in Figure 6a. Once the plating onset is detected (marked with T1), the controller sends a CAN message to the Maccor to reduce the charge rate to 1.25C.

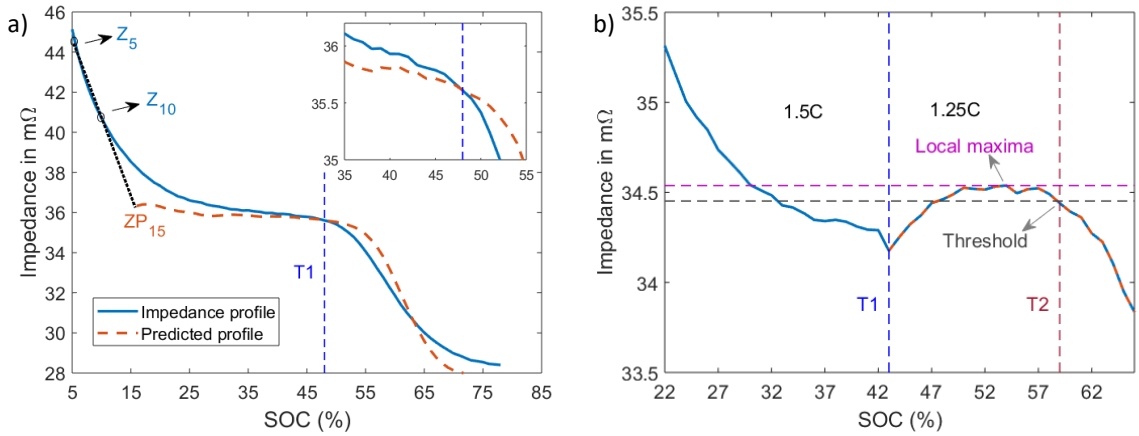

Figure 6: Online detection of plating onset: a) Onset is marked with T1 at 1.5C and b) T2 at 1.25C

After the first charge rate reduction from 1.5C to 1.25C, a different approach is used to detect the onset of plating as the number of impedance values acquired at the early part of the new CC stage (≤ 1.25C) are not sufficient enough to apply the prediction. The peak level of the impedance is recorded as the impedance starts to rise and plating onset is identified if the current impedance level drops by more than 0.3% from the peak. Figure 6b shows how this approach works when applied on the impedance data collected at the 1.25C CC stage of an OFF2 cell. As seen from the figure, impedance increased in the initial phase of 1.25CC stage to reach a peak level of 34.57 mΩ before it started to drop. When a drop of 0.3% (to 34.4 mΩ) from the peak is detected, the negative trend is detected and a transition to the next lower CC rate (marked as T2) is issued. This approach is followed similarly for all other lower CC stages in the online approach until the cell voltage reached 4.2 V.

4. Results and Discussion

4.1 Performance of the proposed charge profiles

Optimized charging profiles are required to simultaneously minimize charging time and degradation associated with the use of fast charging. Use of a high current to reduce the charge time with the standard CC-CV profile can lead to lithium plating and therefore accelerated ageing. As discussed within [9], the SOC level at which plating commences can vary according to the operating temperature, charge rate and ageing level. The onset of plating can be identified from the impedance profiles as described in the offline pre-characterization procedure which can be used as a trigger to initiate a charge current transition from a higher to a lower level.

The offline profile with the multi-stage CC protocol is derived from the pre-characterization procedure that identified the transition voltages for each CC stage (section 3.2). For the online profile, the transitions are identified as the charge progresses for each CC charge stage. These charge profiles (online and offline) are evaluated while cycling the cells and compared with the standard CC-CV charging profile. The results of the cycle ageing test with the charging protocols at 20^{o}C are summarized in Figure 7. The standard CC-CV protocol with a 1C charge rate is found to result in the highest level of degradation. Figure 7 a and b show the state-of-health (SOH) as a function of cycle number and Ah throughput, respectively. Here, SOH is defined as the ratio of the current capacity vs the nominal value when the cell was new. The proposed multi-stage CC charging procedures show significantly higher charge throughputs compared to the respective standard CC-CV charging protocol. The online and offline approaches allow total throughputs for the used

18650 cells for 340 and 635 Ah, respectively while staying above 80% SOH. In contrast, the standard CC-CV charging protocol at 1C leads to a total charge throughput of only 194 Ah by the time it reaches 80% SOH.

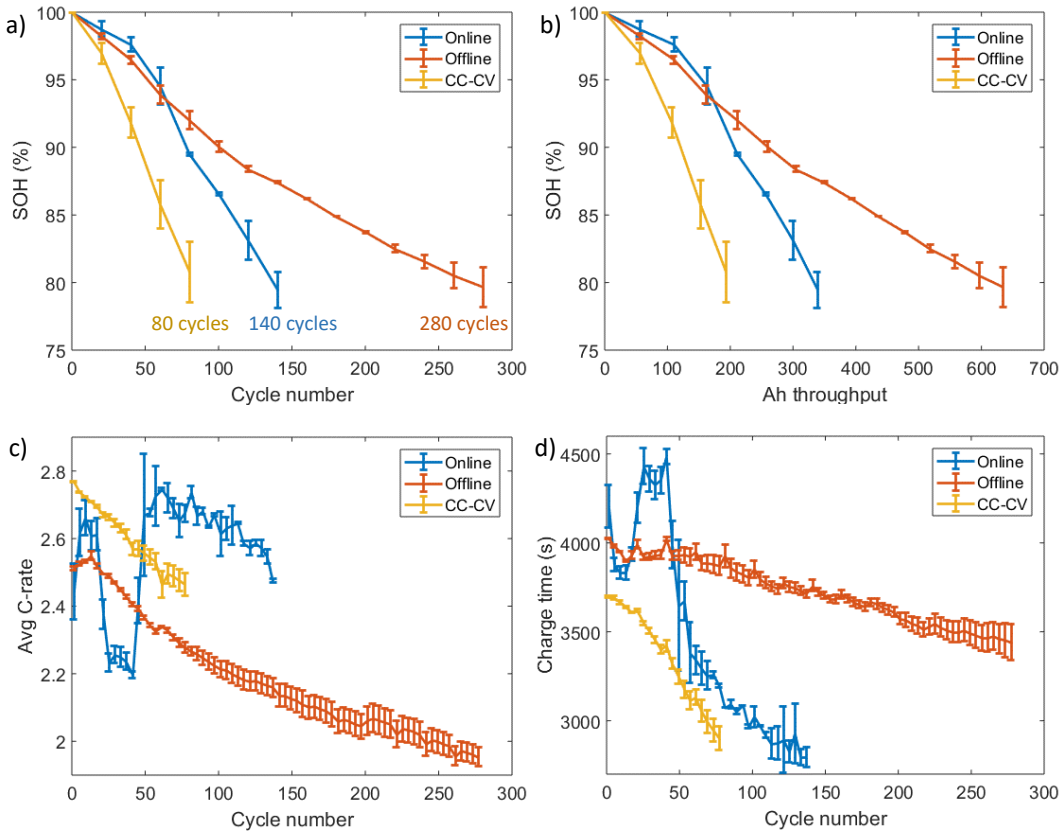

Figure 7: Comparison of different charging strategies: SOH as a function of a) cycle number and b) Ah throughput; c) average charging C-rate and d) charging time as a function of cycle number.

While comparing the charging speed, increased charging time or reduced average charge C-rate up to 20% is observed for the proposed charge profiles compared to that of the CC-CV protocol as shown in Figure 7c and d. The offline profile compared to the CC-CV took circa 8.5% higher charging time (4025 s against 3711 s) at cycle number one which gradually increased to a 19% difference (3450 s 2900 s) by the time they reached their respective 80% SOH levels. The cells in the online profile experienced similar levels of charging speed at the start of the cycling that reduced by nearly 10% in middle (cycle number 40) before finally, it became circa 20% faster in the end compared to the offline protocol. The reason for this is that the online approach adapts to the changes occurring as the battery age whereas the offline method uses fixed voltage levels for the charge rate transitions. Between 20 and 45 cycles, the charging speed reduced in the online approach because of the shorter mid CC stages (e.g. 1.25 to 0.75C). After 45 cycles, the charging speed started to rise as the charge addition in the mid CC stages increased.

To make the comparison more understandable, given that charging time and SOH are changing with cycle number; the average charging time and cycle number (for a capacity reduction of 20%) are shown in Table 5. At the cost of circa 4% higher charging time, the online profile could extend the cycles by 75% compared to that of the CC-CV profile. Whereas the cell with the offline profile took an average 13% longer charging time while prolonging the cycle life by 250% compared to that of the cells with the CC-CV profile.

Table 5: Comparison of three charge profiles

Profile	Average charge time (s)	Number of cycles to lose 20% capacity
CC-CV	3310	80
Online	3440	140
Offline	3750	280

Figure 8a to c show the impedance profiles of the charging profiles at different cycle numbers. The star marks in the figures indicate the charge rate transitions for the proposed charge profiles. As seen from Figure 8a, at 1C stage, charge capacity addition is increased from circa 0.3 Ah at 21st cycle to 0.75 Ah in the 61st cycle. Therefore, with the increased capacity addition at high C-rates, overall charging time is reduced. Increased time between the actual onset (where the impedance rise slows down) to the detectable level (where the impedance drops by 0.3% from the peak level) at mid CC stages could extend the mid-CC stages. This shows that the rate at which the impedance profile deviates tends to reduce with increasing battery ageing and suggests that the rate at which lithium plating rises after its onset is reducing with ageing. This could occur if the influence of degradation on the CTL faced by the plating reactions is higher than that of the intercalation reactions. However, such a conclusion needs further study to understand the impact of previous lithium plating influence on the competing reactions in the form of lithium plating and lithium intercalation into the graphite.

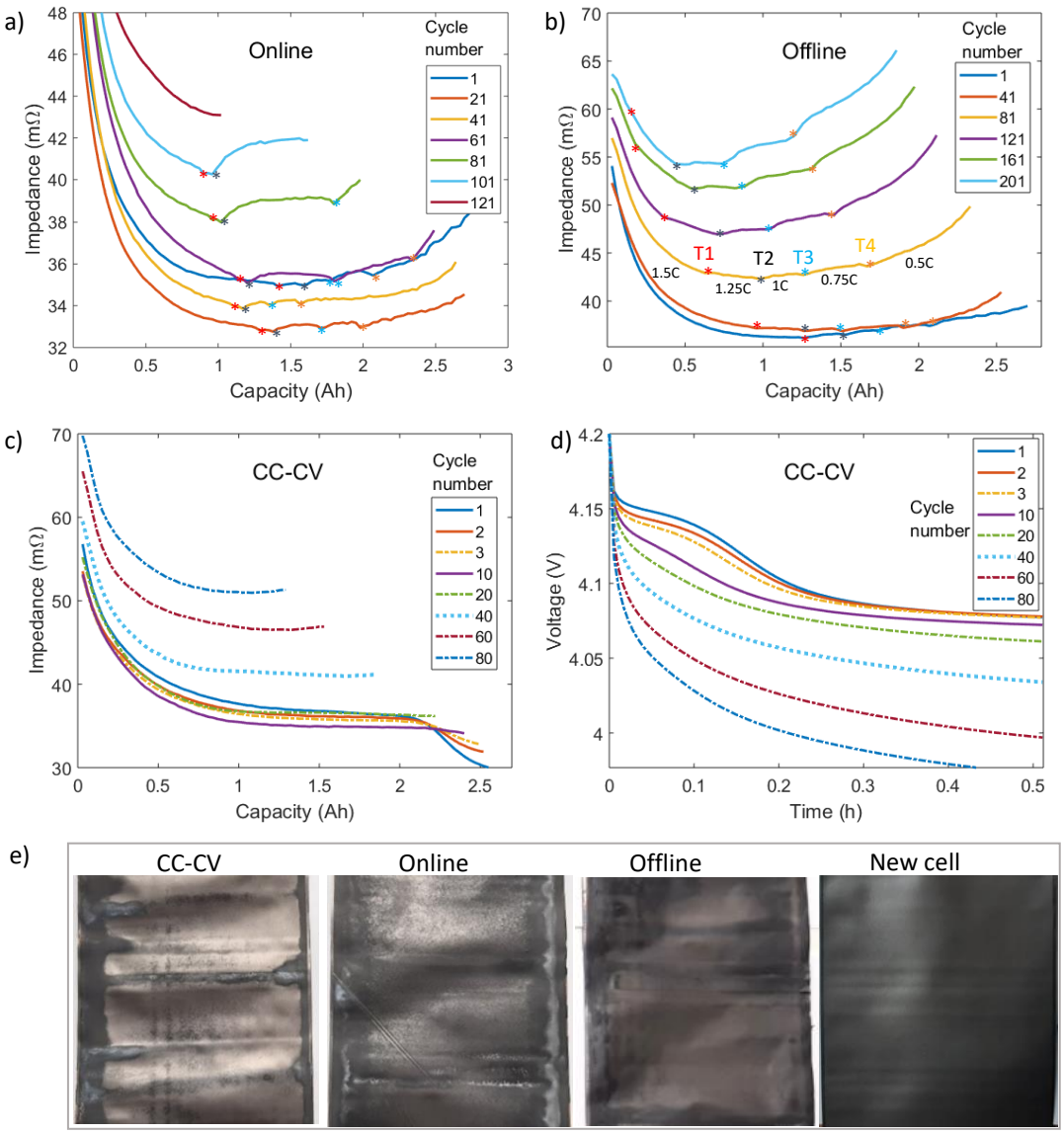

Figure 8: Comparison of charging strategies: Impedance profiles of a) online, b) offline and c) CC-CV protocols as a function of charge capacity, d) voltage relaxation profiles of the CC-CV protocol and e) visual inspection of graphite electrodes separated from aged cells under different protocols and a new cell.

The improvement in the cycle life in both offline and online approaches compared to the CC-CV profile can be explained through the impedance profiles derived in each charging event. As seen from Figure 8a and b, the impedance profiles in the proposed strategies avoid large second negative trends that, in turn, reduce lithium plating amounts. While Figure 8c shows the impedance profiles for a cell using the traditional CC-CV profile that shows a second negative trend inferring large amounts of lithium plating particularly up to the first 20 cycles. Figure 8d shows the post-charge voltage relaxation profiles for the same cell that exhibit a two-stage relaxation in the first twenty cycles. As described in [6, 23], lithium plating that introduces a new phase to the graphite potential tends to produce a characteristic two-stage voltage relaxation profile at the cell level. On the other hand, none of the cell voltage profiles in post-charge relaxations is found with a two-stage relaxation for both the proposed protocols indicating lithium plating levels are below the detectable levels (approximately <2.5%). Therefore, impedance and VRP methods together indicate higher levels of lithium plating

with the CC-CV protocol. Avoiding large negative trends (as seen from Figure 8a and b) both in offline and online approaches could minimize the plating depositions and result in improved battery life.

4.2 Cell inspection

One cell from each protocol was randomly selected to open to visually inspect metallic depositions on the graphite electrode surface. For comparison, a new cell is also dismantled. The cells were opened in an argon-filled glove box and electrodes are inspected visually for metallic depositions [27]. Figure 8e shows images of the graphite electrodes of the new cell and the cells selected from the CC-CV, online, and offline protocols. The graphite electrode of the new cell appears mostly black, as expected for a functional fully discharged graphite-based electrode [8]. A few areas exhibiting silvery depositions are found on the graphite electrode of the offline cell. Meanwhile, much larger and distinguished areas with silver colour depositions are observed for the online cell. On the other hand, the NE of the CC-CV cell exhibits relatively highest dense silver colour depositions compared to other cells. As discussed within [8, 27], since the graphite electrode does not appear in silver colour at any of its lithiation levels, these depositions can be attributed to lithium plating. It is asserted therefore that proposed charge protocols are able to reduce the lithium plating levels when compared to the CC-CV protocol. Between the proposed protocols, lithium plating depositions are found to be higher with the online protocol compared to the offline approach.

The approach adopted in the derivation of proposed charge profiles cannot completely avoid lithium plating. After the first transition to 1.25C as shown in Figure 6b, the impedance starts to rise in this initial stage and then the rate of increase starts to slow down towards zero before turning to negative levels. The rate of Impedance rise slowing could occur due to the onset of plating. In this case, there could be a small amount of plating by the time rate of change in the impedance becomes zero and some more with as the impedance starts to drop. The use of a zero rate of change or negative rate of change can cause a small amount of plating. In the offline approach, the cell voltage corresponding to the impedance rate reaching the zero level is defined as the transition point. While the online approach identifies the transition when the impedance drops from the peak level by 0.3% where the impedance rate of change is already turned to negative from the zero levels. Therefore a small amount of plating could occur in each cycle in the proposed charge protocols with online procedure having higher levels compared to the offline one.

4.3 Online control in partial charge events

To further understand the transferability of the online control approach to real-world applications, the control procedure detailed in Section 3.2 is verified in cases where cells are not fully discharged. Before the partial charge events, a set of new cells that are fully discharged to 2.5 V are charged at C/3 to different starting SOC levels (20, 40, 50, 60 and 70%) and then allowed to rest for 4 h. After this, the cells are charged with the online charge control (beginning with 1.5C) to understand the online control behaviour under partial charge events. Figure 9 shows the impedance profiles for these charging events.

According to the online procedure, a minimum of 10% capacity addition or previous ten impedance values is needed for detecting the onset. For the case of 60% SOC level at the start point, the impedance started to drop as soon as the charge initiated and the drop accelerated significantly after the first 5% capacity addition. As seen from Figure 9, the 0.42 mΩ drop in the first 5% SOC rise is increased to circa 1.9 mΩ in the next 5% SOC rise. The accelerated reduction in the impedance level at SOC levels higher than 60% indicates the presence of lithium plating. However, as the designed algorithm begins to verify the onset of plating after a minimum of 10% SOC increase irrespective of the SOC level at the beginning of the charge, the onset is identified after the SOC is reached 70%. Therefore, the delayed detection of the onset could result in increased levels of lithium plating. While for the SOC start levels 50% or lower, the impedance-based control can minimize negative drop and could control the profile with the identified transition points. In the case of 70% as the SOC start level, the cell reached 4.2V in less than 2 minutes with the 1.5C charge rate. Therefore, the results indicate that online procedure may fail to limit lithium plating levels in partial charge events and, as discussed in section 5.1, needs further refinement.

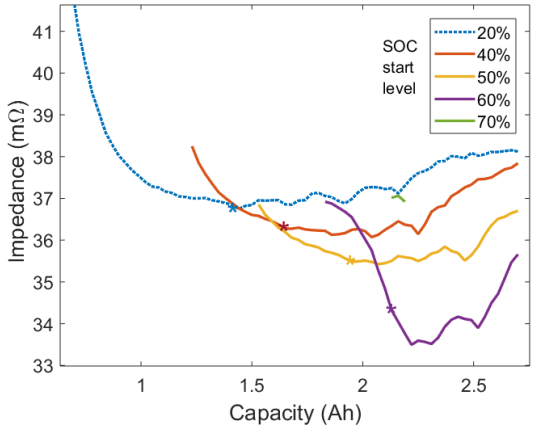

Figure 9: Impedance profiles at different partial charge events. Star marks indicate the first transition from 1.5C to 1.25C.

4.4 Lithium plating occurrence as cell ages

As seen from Figure 8c, the impedance profiles of the CC-CV charge have shown the second negative trend until the first 20 cycles although the magnitude of the impedance reduction in the second negative trend is reducing with cycle number. From circa 7 mΩ or 20% drop in the first cycle, the impedance drop in the second negative trend is reduced nearly to zero by the 20th cycle and no negative trend is observed thereafter. The reason for the undetected lithium plating occurrence beyond 20 cycles can originate from one of two reasons. First, as discussed within [19], there is a possibility of reducing lithium plating levels with the cycle number and then no significant levels of plating in further cycles. With the large levels of lithium plating in the initial cycles as detected with the impedance profiles and VRP method (see Figure 8c and d), plating tendency may reduce in the latter cycles. With the loss of cyclable lithium to the plating depositions and subsequent SEI layer growth in the presence of metallic lithium depositions can reduce the SOC level and the lithiation levels of the NE towards the end of CC charge. As seen from Figure 8c, the SOC level towards the end of CC charging has reduced from 84% (2.52 Ah against the total capacity of 3.12 Ah) in the first cycle to 52% (1.29 Ah against 2.48 Ah) in the 80th cycle. The increased potential drops could increase the cell voltage to 4.2 V in the CC phase at a much a lower SOC level than that of a new cell because of the reduced kinetics associated with battery

degradation in the current collectors, electrodes, electrolyte, SEI layer and charge transfer limitations at the electrode surface. Therefore, although lithium plating could begin, reduced levels of charge in the CC stage may not allow lithium plating levels to rise to the detectable level (> 2.5%).

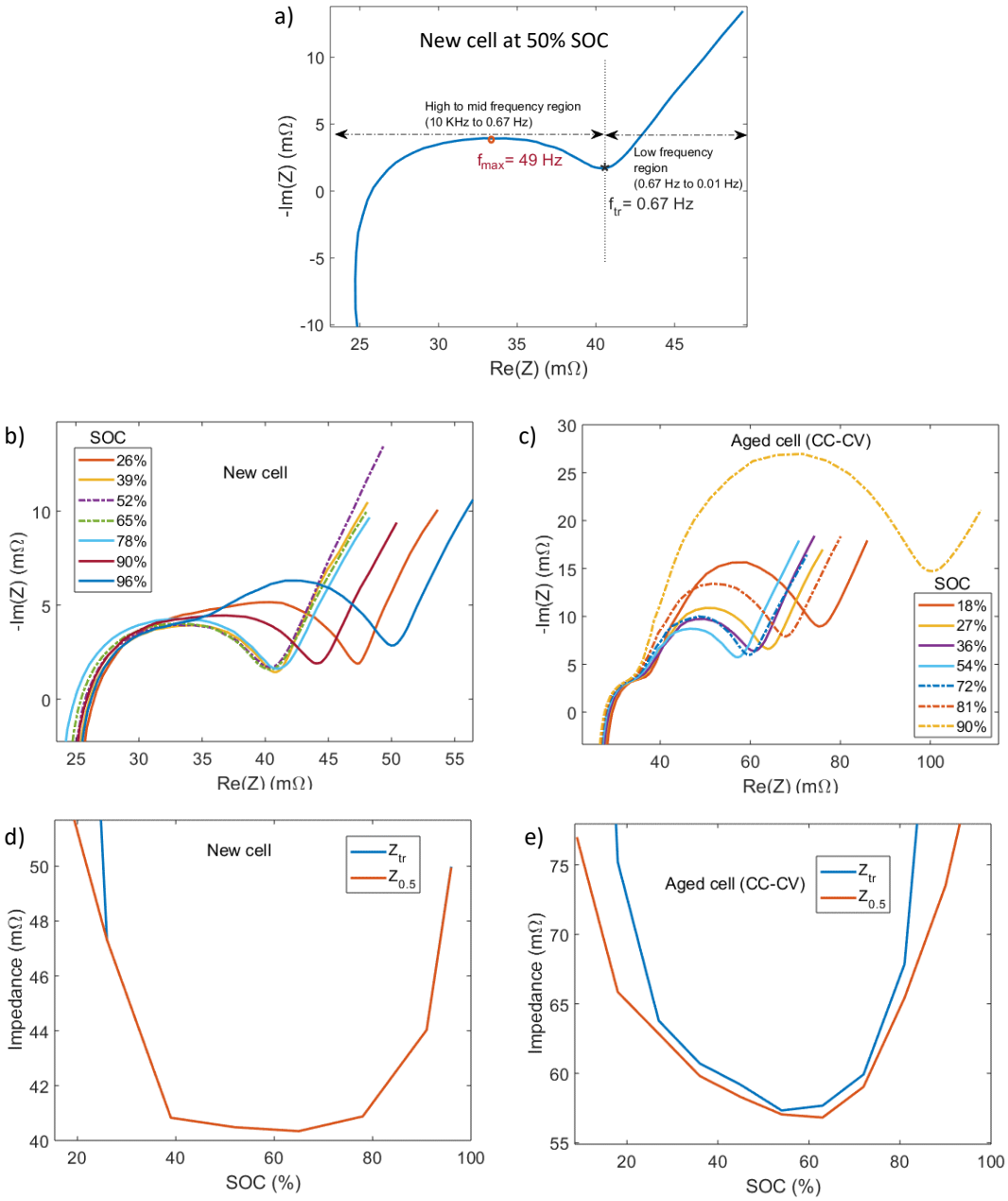

Figure 10: Impedance analysis with the EIS plots: a) EIS plot of a new cell at 50% SOC marked with f_{max} and f_{tr}, EIS plots at different SOC levels for b) a new cell and c) an aged cell; Impedance calculated with 0.5 s interruption and at f_{tr} for d) the new cell and e) the aged cell.

Second, there is a possibility of the impedance method failing to detect plating as the battery ages. The fixed interruption period of 0.5 s derived using new cells may fail to track the impedance as the battery ages. EIS plots at different SOC levels of a new cell and a cell aged under the CC-CV protocol are analyzed to study the influence of the interruption time on the impedance profile tracking. The IT method tracks the impedance at the transition frequency (f_{tr}) where impedance due to diffusion with a slope of 45° begins. To identify the impedance corresponding to f_{tr} with the

interruption procedure, the frequency (f_{max}) at which reactance (imaginary part of the impedance) attains a maximum level in the semicircle region is used. Figure 10a shows the EIS plot of a new cell at 50% SOC level marked with f_{max} and f_{tr}. As discussed within [28], from the f_{max}, the time constant ($\tau = (2\pi f_{max})^{-1}$) of the equivalent RC network that produces a semicircle impedance plot can be identified. Although f_{max} is varying with SOC, a constant period of 0.5 s is considered based on the previous study of a fresh cell since it was able to produce the impedance profile similar to the one captured at the f_{tr}. Since f_{max} reduces and thus τ rises as the cell ages compared to that of a new cell, the impact of constant charge interruption period on the ability to capture the impedance profile is analyzed. An interruption time of 4τ shall produce a voltage recovery of circa 98% of the total recovery. Use of an interruption time smaller than 4τ only allows a portion of total voltage recovery and therefore the impedance calculated (Z_t) shall also indicate a portion of the total impedance (Z_{tr}) as shown here:

$$Z_t = Z_{tr} * (1 - e^{-t/\tau}) \qquad (2)$$

Figure 10b and c show the EIS plots at different SOCs for a new cell and a cell that reached 80% SOH levels with the CC-CV protocol, respectively. From these EIS plots, Z_{tr} and $Z_{0.5\ s}$ profiles for these cells are plotted as shown in Figure 10d and e. For the new cell, Z with 0.5 s interruption is sufficient to track the Z_{tr} (Figure 10d). On the other hand, for the aged cell, the 0.5 s interruption can capture the Z_{tr} profile with up to 20% lower values. However, as discussed within [25], tracking the Z_{tr} profile is sufficient to detect the occurrence of lithium plating. Therefore, the 0.5 s interruption time used for tracking the Z_{tr} may not be the reason behind the non-observation of plating with the impedance method and indicates that lithium plating is reducing with the cycle number.

The reason for continued capacity loss after the first twenty cycles where lithium plating is not detected can occur because of the previously deposited lithium metal. As discussed within [29], lithium metal occupies nearly four times more volume than the volume change due to the lithiation of the graphite. Second, the metal depositions that damage the SEI layer can result in the further regrowth of the SEL layer. As a result, the depositions due to the SEI layer could rise significantly in the presence of plating. Both these depositions could raise the volume expansion and therefore can increase the mechanical stresses locally. As a result, active material cracking and subsequent growth of the SEI layer may continue to occur. This indicates that lithium plating may have a long-lasting impact on battery degradation.

In summary, the analysis presented here indicates that lithium plating is reducing as the cell degrades under the influence of lithium plating in the previous cycles. Therefore plating could not be detected with the impedance method in the later part of cycling. Further, small amounts of plating in each cycle combined with the effect of previous lithium metal depositions and their effect on the SEI layer may continue to degrade the battery.

5. Conclusions and future work

5.1 Future work

5.1.1 Improvement of the proposed strategies

The proposed strategies although they significantly extended the battery life can be further improved concerning the identification of the transition cell voltage levels that correspond to the potential onset of lithium plating. For example, the offline approach infers the onset point to the impedance differential when it reaches zero before it becomes negative. However, as discussed in section 4.2, the actual onset of plating could begin earlier somewhere close to the point where impedance rise starts to slow down. The approach used for identifying the transition could allow small amounts of plating. Such small levels of plating over several cycles may increase battery degradation compared to a low C-rate charge event. Since the Low C-rate shows a continuously rising impedance differential, initiating the transition as soon as impedance rise starts slows down may bring down the lithium plating amounts further. Use of the CE method along with the IT method may allow refining the onset detection accuracy of the IT method. Therefore, further work is required to improve the plating onset identification accuracy and study its impact on battery performance in terms of life and charging speed. In that work, a plating free charge rate such as the manufacturer`s recommended C-rate will be included as an additional test case in life tests for improved comparison of the proposed charge protocols.

5.1.2 Charging strategy selection

The experimental work presented indicates that the offline protocol is better in extending the battery life while the online is superior for improving the charging speed. The predefined charge profile used in the offline approach could cause small amounts of lithium plating in the early cycle as discussed in 5.1.1 and avoid lithium plating completely in later cycles as lithium plating tendency reduces with increased cycles as detailed in Section 4.4. Conversely, the online approach that modifies the charge profile when it detects lithium plating could induce a small amount of lithium plating in every cycle thus apply high CC charge for a longer time and lose the capacity faster compared to the offline approach. To trade-off between battery life and charging speed, both the approaches can be incorporated into a charging strategy to adapt the offline profile to battery ageing. Therefore, further study is needed in these areas to facilitate future deployment of fast charge algorithms.

5.1.3 The long-lasting impact of the plating

As observed in this work, the cells with the CC-CV charge protocol have experienced large levels of lithium plating which are then reduced with the increasing cycle number. However, the cells experienced higher levels of degradation in the later cycles where plating is not detected. One possibility is that depositions from the lithium plating in the early cycles might impact the battery kinetics and capacity fade. In such a context, lithium plating occurrence in the batteries needs to be completely avoided to eliminate the long-lasting negative impact of previous lithium depositions. To identify the reasons behind the higher levels of degradation in the later cycles where plating is not detected using the IT method, further work is required. In that work, lithium-plating tendency and the detection ability of the IT method in cells aged in different operating conditions need to be further verified.

5.1.4 Charging strategy for partial charge events

The current derivative of the online approach is failing to detect and limit the plating occurrence when the starting SOC level is already high. Since even small amounts of plating in a few charging events may cause considerable degradation, Online control in the first 10% SOC rise needs further improvement. For example, a comparison of the rate of change as SOC rises may provide further information in addition to the extrapolation of impedance profile. Further, SOC or voltages levels identified for each transition in full charge events can be recorded and used in partial charge events as hard limits in case of no sufficient data in the current charging event is available. Further work is required to improve Online control.

5.2 Conclusions

The impedance-based lithium plating detection method is utilized in developing two different charging strategies- online and offline. An iterative pre characterization procedure is proposed to derive the offline charging profile with the multi-stage CC charge protocol. On the other hand, an online control algorithm is developed for a TI controller to detect the onset of lithium plating and reduce the charge current in the online strategy.

The experimental results indicate that a significant improvement in battery life (lithium plating reduction) could be achieved by implementing the proposed methods. The online and offline could approach with up to 20% increase in the charging time can extend the battery life by circa 75% and 250%, respectively compared to the CC-CV protocol before losing a 20% capacity.

The analysis along with the inspection of electrodes after the ageing tests indicates that proposed charge profiles do reduce lithium plating. The presented approach that identifies the onset of lithium plating allows small levels of lithium plating in each cycle and it can be improved to reduce lithium plating levels further. A proactive approach of reducing the charge current as soon as the impedance rate of rising starts to reduce instead of waiting until it starts to drop may reduce those small levels of plating occurrence in each cycle. Therefore, further work is needed to improve the proposed strategies. In such a study, the impact of the modified charge profile on the charging performance can be evaluated to provide a trade-off analysis between the charging speed and battery life.

References

1. Anseán, D., et al., *Fast charging technique for high power lithium iron phosphate batteries: A cycle life analysis.* Journal of Power Sources, 2013. **239**: p. 9-15.
2. Park, H., et al., *Thermal Behavior of Solid Electrolyte Interphase Films Deposited on Graphite Electrodes with Different States-of-Charge.* Journal of the Electrochemical Society, 2015. **162**(6): p. A892-A896.
3. Pinson, M.B. and M.Z. Bazant, *Theory of SEI Formation in Rechargeable Batteries: Capacity Fade, Accelerated Aging and Lifetime Prediction.* Journal of the Electrochemical Society, 2012. **160**(2): p. A243-A250.
4. Saulnier, M., et al., *Manganese dissolution in lithium-ion positive electrode materials.* Solid State Ionics, 2016. **294**: p. 1-5.
5. Birkl, C.R., et al., *Degradation diagnostics for lithium ion cells.* Journal of Power Sources, 2017. **341**: p. 373-386.
6. von Lüders, C., et al., *Lithium plating in lithium-ion batteries investigated by voltage relaxation and in situ neutron diffraction.* Journal of Power Sources, 2017. **342**: p. 17-23.

7. Frisco, S., et al., *Understanding Li-Ion Battery Anode Degradation and Pore Morphological Changes through Nano-Resolution X-ray Computed Tomography.* Journal of The Electrochemical Society, 2016. **163**(13): p. A2636-A2640.
8. Gallagher, K.G., et al., *A Volume Averaged Approach to the Numerical Modeling of Phase-Transition Intercalation Electrodes Presented for LixC6.* Journal of the Electrochemical Society, 2012. **159**(12): p. A2029-A2037.
9. Waldmann, T., M. Kasper, and M. Wohlfahrt-Mehrens, *Optimization of Charging Strategy by Prevention of Lithium Deposition on Anodes in high-energy Lithium-ion Batteries – Electrochemical Experiments.* Electrochimica Acta, 2015. **178**: p. 525-532.
10. Koleti, U.R., et al., *The development of optimal charging strategies for lithium-ion batteries to prevent the onset of lithium plating at low ambient temperatures.* Journal of Energy Storage, 2019. **24**.
11. Ren, D., et al., *Investigation of Lithium Plating-Stripping Process in Li-Ion Batteries at Low Temperature Using an Electrochemical Model.* Journal of The E lectrochemical Society, 2018. **165 (10) A2167-A2178**
12. Ge, H., et al., *Investigating Lithium Plating in Lithium-Ion Batteries at Low Temperatures Using Electrochemical Model with NMR Assisted Parameterization.* Journal of The Electrochemical Society, 2017. **164**(6): p. A1050-A1060.
13. Varini, M., P.E. Campana, and G. Lindbergh, *A semi-empirical, electrochemistry-based model for Li-ion battery performance prediction over lifetime.* Journal of Energy Storage, 2019. **25**.
14. Anseán, D., et al., *Operando lithium plating quantification and early detection of a commercial LiFePO 4 cell cycled under dynamic driving schedule.* Journal of Power Sources, 2017. **356**: p. 36-46.
15. Guo, Z., et al., *Optimal charging method for lithium ion batteries using a universal voltage protocol accommodating aging.* Journal of Power Sources, 2015. **274**: p. 957-964.
16. Burns, J.C., D.A. Stevens, and J.R. Dahn, *In-Situ Detection of Lithium Plating Using High Precision Coulometry.* Journal of the Electrochemical Society, 2015. **162**(6): p. A959-A964.
17. Zou, C., et al., *Electrochemical Estimation and Control for Lithium-Ion Battery Health-Aware Fast Charging.* IEEE Transactions on Industrial Electronics, 2018. **65**(8): p. 6635-6645.
18. Hu, X., et al., *Optimal Multistage Charging of NCA/Graphite Lithium-Ion Batteries Based on Electrothermal-Aging Dynamics.* IEEE Transactions on Transportation Electrification, 2020. **6**(2): p. 427-438.
19. Petzl, M., M. Kasper, and M.A. Danzer, *Lithium plating in a commercial lithium-ion battery – A low-temperature aging study.* Journal of Power Sources, 2015. **275**: p. 799-807.
20. McTurk, E., et al., *Thermo-electrochemical instrumentation of cylindrical Li-ion cells.* Journal of Power Sources, 2018. **379**: p. 309-316.
21. Zinth, V., et al., *Lithium plating in lithium-ion batteries at sub-ambient temperatures investigated by in situ neutron diffraction.* Journal of Power Sources, 2014. **271**: p. 152-159.
22. Petzl, M. and M.A. Danzer, *Nondestructive detection, characterization, and quantification of lithium plating in commercial lithium-ion batteries.* Journal of Power Sources, 2014. **254**: p. 80-87.
23. Schindler, S., et al., *Voltage relaxation and impedance spectroscopy as in-operando methods for the detection of lithium plating on graphitic anodes in commercial lithium-ion cells.* Journal of Power Sources, 2016. **304**: p. 170-180.
24. Koleti, U.R., et al., *A new concept to improve the lithium plating detection sensitivity in lithium-ion batteries* International Journal of Smart Grid and Clean Energy 2019. **vol. 8, no. 5**: p. 505-516.
25. Koleti, U.R., T.Q. Dinh, and J. Marco, *A new on-line method for lithium plating detection in lithium-ion batteries.* Journal of Power Sources, 2020. **451**.
26. Barai, A., et al., *A study on the impact of lithium-ion cell relaxation on electrochemical impedance spectroscopy.* Journal of Power Sources, 2015. **280**: p. 74-80.
27. Bach, T.C., et al., *Nonlinear aging of cylindrical lithium-ion cells linked to heterogeneous compression.* Journal of Energy Storage, 2016. **5**: p. 212-223.

28. Waag, W., S. Käbitz, and D.U. Sauer, *Experimental investigation of the lithium-ion battery impedance characteristic at various conditions and aging states and its influence on the application.* Applied Energy, 2013. **102**: p. 885-897.
29. Bitzer, B. and A. Gruhle, *A new method for detecting lithium plating by measuring the cell thickness.* Journal of Power Sources, 2014. **262**: p. 297-302.